Science & Global Security, 22:209–234, 2014

ISSN: 0892-9882 print / 1547-7800 online
DOI: 10.1080/08929882.2014.952581

Routledge
Taylor & Francis Group

Determination of the Global Coverage of the IMS Xenon-133 Component for the Detection of Nuclear Explosions

Michael Schoeppner[1,2] and Wolfango Plastino[2,3]

[1]Institute for Peace Research and Security Policy, University of Hamburg, Hamburg, Germany
[2]Department of Mathematics and Physics, Roma Tre University, Rome, Italy
[3]National Institute of Nuclear Physics, Roma Tre University, Rome, Italy

Radioxenon is an important atmospheric tracer to detect underground nuclear explosions. The International Monitoring System is designed to provide worldwide continuous physical monitoring and detection of nuclear explosions and incorporates 40 noble gas monitoring stations. They are constantly sampling the atmosphere for concentrations of radioxenon. This work analyses how effectively the network of stations is able to detect unusual xenon-133 concentrations in the atmosphere. A large multitude of nuclear explosions, evenly distributed in space and time, is simulated and the detection rate is calculated. Atmospheric transport modelling is applied to calculate the source-receptor-sensitivities for each monitoring station. The approach includes the anthropogenic radioxenon background, station-specific detection criteria, different scenarios for surface and subsurface nuclear explosions, and a spatial as well as a time dependent analysis. Recommendations are drawn for the improvement of the detection capability.

INTRODUCTION

Nuclear test explosions are an important instrument for states to develop new types or configurations of nuclear weapons and to maintain existing weapon arsenals, e.g., against aging effects. Beyond that nuclear weapon tests can be potentially used by states for political means to demonstrate their nuclear and

Received 18 December 2013; accepted 7 July 2014.
Address correspondence to Michael Schoeppner, Program on Science and Global Security, Princeton University, 221 Nassau Street, Princeton, NJ 08542, USA. E-mail: schoeppner@princeton.edu
Color versions of one or more of the figures in the article can be found online at www.tandfonline.com/gsgs.

technical capabilities. On the other hand it is imaginable that a state is going to secretly test a nuclear weapon, but does not want the world public to know about it. Thus, three scenarios are conceivable: (a) an open test, when a state tests a nuclear bomb and publicly admits it, (b) a secret test, when a state tests a nuclear bomb, but does not admit it, and (c) a fake test, when a state conducts a conventional/chemical explosion and claims it to be nuclear. Observed from the outside these scenarios cannot be necessarily distinguished. The true nature of an event must be independently assessed not from a political but a physical point of view to provide a sound basis for decision making by the international community.

In 1996 the international community opened the Comprehensive Nuclear-Test-Ban Treaty (CTBT) for signature. According to the current wording it will, once it has entered into force, forbid all ratifying member states to conduct or allow a nuclear explosion within their control. The treaty text foresees that it will only enter into force once all 44 countries that are listed in Annex-2 of the treaty have ratified it. These 44 countries are those which had access to nuclear technology during the treaty's opening for signature. The eight remaining Annex-2 states that have not yet ratified the treaty are the United States, China, Israel, Egypt, Iran, India, Pakistan, and North Korea. Iran, India, Pakistan, and North Korea have not yet signed the treaty.

The reliable verification of the CTBT is an essential factor for its future success and international acceptance. A highly energetic event like a nuclear explosion couples in various ways into the environment, whether it is underground, underwater or atmospheric and provides a range of possibilities for detection.

In order to ensure a comprehensive verification regime the Preparatory Commission of the CTBT Organisation (CTBTO) is building the International Monitoring System (IMS). Its task is the worldwide, continuous physical monitoring and detection of nuclear explosions. The IMS monitors four physical domains: seismic, hydroacoustic, and infrasound waves, and the atmospheric concentration of selected radionuclides. In contrast to the three waveform technologies, radionuclide monitoring has the unique potential to provide empirical data on the nuclear character of an event. As of July 2014, 85 percent of the IMS stations are operational. When all stations are operational the IMS will be comprised of a total of 171 seismic, 11 hydroacoustic and 60 infrasound stations worldwide. The radionuclide component of the IMS is designed with 80 monitoring stations, of which 40 will be equipped with noble gas monitoring and detection equipment to continuously sample the atmospheric concentrations of four radioactive xenon isotopes (and isomers), namely xenon-131m, xenon-133, xenon-133m, and xenon-135. This radionuclide and noble gas component has been designed to provide an estimated 90 percent detection probability within 10 days after a nuclear explosion.[1]

In addition to the IMS, the verification regime of the CTBT includes consultation and clarification, on-site inspections and confidence-building measures.[2]

The current status of signatures and ratifications, the list of Annex-2 states, the locations of the monitoring stations and their status can be viewed online at www.ctbto.org/map.

The radionuclide monitoring system, including its noble gas component, relies on particles or gases to be released from the event into the atmosphere and transported with the prevailing winds until reaching a monitoring station in a diluted concentration. This work applies atmospheric transport modelling to assess the capability of the IMS xenon-133 component to successfully detect nuclear explosions worldwide and gives recommendations on how to improve it.

Noble Gas Detection of Nuclear Explosions

These aforementioned four radioxenon isotopes have been selected due to their suitable characteristics for nuclear explosion monitoring, especially for underground explosions. Their fission yield is sufficiently high; their inert noble gas characteristic allows them to be leaked even from underground cavities into the atmosphere without chemical bonding in the surrounding earth; their half-lives are suitable, i.e., not too long to allow a build-up in the atmosphere leading to a high background against which detection would become more difficult and not too short to decay before reaching a monitoring station; and there is no natural background of radioxenon in the atmosphere, only an anthropological one. Well suited for nuclear explosion monitoring is xenon-133 due to its cumulative fission yield of 5–7 percent (depending on the fissile material and the neutron energy) for uranium and plutonium devices and its half-life of 5.24 days (d).

To detect radioxenon emissions from nuclear explosions, various factors have to be taken into account. The fission yield determines how much radioxenon is produced directly during the fission process. The amount of radioxenon released into the atmosphere is strongly dependent on the environment of the explosion. Once released the gases are transported and diluted in the atmosphere. When arriving at the monitoring station, the particle concentration must exceed the minimum detectable concentration (MDC) of the detector.

For this work relatively small nuclear explosions are assumed, because the monitoring network is aimed at detecting and locating an explosion of 1 kiloton (kt) anywhere in the world. During a nuclear chain reaction that happens throughout such an explosion approximately 10^{13} Bq of xenon-133 is produced initially.[3] After 3 hours the activity reaches about 10^{15} Bq of xenon-133 through ingrowth. The isotope build-up of xenon-133 has its maximum of approximately 10^{16} Becquerel (Bq) between 1 day and 1 week after the event.

For the case of an underground nuclear explosion only a certain amount of the gas reaches the surface and vents into the atmosphere. In other publications, leakages between 1 and 10 percent of the maximum activity are

assumed.[4] Assuming that at some point leakage is taking place, a leakage of 1 percent of the maximum activity, i.e., 10^{14} Bq, is the basis for further calculations in the following.

The atmospheric transport simulations described below uses a time resolution of 3 hours. Thus, for atmospheric explosions a release of 10^{15} Bq/kt is assumed. To further accentuate different scenarios and to get a clearer understanding of the influence of the released activity on the detection probability the emissions from atmospheric explosions are assumed to be 10^{16} Bq, i.e., equivalent to the activity of a 10kt nuclear explosion within 3 hours.

Once they are airborne, the gases follow various trajectories according to the prevailing winds in the atmosphere, which leads to a dilution of the concentration and a dispersion over the globe. The monitoring stations have a typical distance in the order of about 1,000 km from each other. For such distances a typical atmospheric dilution is in the order of 10^{-14} to 1^{-18} m^{-3}.[5] Furthermore, the absolute concentration in the atmosphere declines during the atmospheric transport due to radioactive decay.

The noble gas monitoring stations are equipped either with high-resolution gamma-spectrometers or with beta-gamma coincidence detectors. In high-resolution gamma-spectrometry the radioxenon isotopes are detected and quantified with a high-purity germanium (HPGe) detector by their distinctive gamma lines. In beta-gamma coincidence systems a plastic scintillator tube for beta detection is surrounded by a NaI(Tl) gamma detector.[6] Applying coincidence measurements significantly reduces the background. For the IMS monitoring stations the systems with high-resolution gamma spectrometry have a sampling time of 24 hours, while the beta-gamma systems have a sampling time of 12 hours. The design specifications of the IMS foresee a MDC of 1 mBq/m^3 for xenon-133. Depending on the installed system a MDC of 0.4–0.6 mBq/m^3 can be reached.[7]

According to the CTBT a total of 40 noble gas monitoring stations are planned. However, as of July 2014, only 39 stations have been allocated; the 40th station is supposed to be located in India, but is still subject to negotiations. Fifteen of these 39 stations are already certified for continuously taking data; another 15 have been installed and are running, while awaiting certification; ten are currently in planning or under installation. However, the successful xenon-133 detection of nuclear explosions also depends on the manmade, atmospheric xenon-133 background, which is discussed in the following section.

Xenon-133 Background Sources

As mentioned before, the four selected radioxenon isotopes have no natural background sources. They are created in significant quantities in nuclear reactions, such as fission of heavy nuclei, e.g., uranium-235, or nuclear

reactions such as (n,p) reactions.[8] All four relevant radioxenon isotopes are created in significant yields in fission induced by thermal (i.e., slow) neutrons. Apart from xenon-131m the other three isotopes also have significant yields, when fission is induced by fission-originated (i.e., fast) neutrons. Thermal neutron induced fission is the major reaction in nuclear reactors, while fast fission occurs in nuclear explosions. Significant emissions are released from a medical isotope production facility (IPF) or a nuclear power plant (NPP). To a lesser degree, emissions from research reactors, reprocessing plants, hospitals, nuclear driven ships and submarines, are contributing to the global background, but are either emitting too irregularly and/or at too small quantities to be considered.[9] Therefore, in the following analysis only emissions from IPFs and NPPs are considered when determining the impact on the IMS xenon-133 component.

In terms of xenon-133 releases the IPFs are clearly the strongest emitters with 10^{11}–10^{13} Bq/d. However, only few of them exist in the world; it is a business sector with few actors who are supplying the world's demand in medical isotopes. For this work the calendar year of 2010 has been considered, for which five operating IPFs have been taken into account. These are located in Sydney (Australia, 5×10^{14} Bq/a), Fleurus (Belgium, 10^{15} Bq/a), Chalkriver (Canada, 10^{16} Bq/a), Petten (Netherlands, 7×10^{11} Bq/a), and Pelindaba (South Africa, 4×10^{15} Bq/a). Their typical emission strengths averaged over 1 year have been gathered from other publications,[10] at conferences,[11] or during personal communication.[12]

Typically operating NPPs have much lesser emissions of xenon-133 when compared to IPFs, but their worldwide occurrence is much higher. In 2007 a total of 439 power reactors were in operation at 195 sites. They are mainly located in East Asia, Europe, and North America. Their typical emissions of xenon-133 average about 10^9 Bq/d. For each individual NPP site the average annual releases of xenon-133 have been gathered, calculated, or estimated.[13] According to the Power Reactor Information System (PRIS) of the International Atomic Energy Agency (IAEA) the total number of power reactors in operation has not changed significantly from 2007 to 2010.[14] The low numbers of new or shut down reactors is negligible for this work due to the low emissions from NPPs compared to IPFs. The background is characterized by a few strong sources (IPFs) and many weak sources (NPPs), where a typical IPF releases as much radioxenon per time as all NPPs combined.

For this work a database of operating IPFs and NPPs has been compiled with information about the average annual xenon-133 releases assumed for each facility in the year of 2010 and the location on a latitude-longitude grid with a one-degree resolution. As previously discussed, the global distribution of xenon-133 emitting facilities has strong concentrations in East Asia, Europe, and North America, which leads to a heterogenic background of xenon-133 concentrations. This background mainly depends on the emission

strength of each facility, its location, and the prevailing winds and meteorological patterns. Consequently the experimental experience shows that each noble gas monitoring station has a different and fluctuating background concentration of xenon-133, depending on its location, the meteorological situation of that time, and any upwind emissions of xenon-133.

This background from sources such as IPFs and NPPs is considered as a legitimate background, whereas a contribution from a nuclear explosion is considered as an unusual, additional concentration that has to be identified. The particular and fluctuating background at each monitoring station can make it difficult to successfully identify the contribution from a nuclear explosion. Naturally this is easier for monitoring stations with low or usually no background. Atmospheric transport modelling (ATM) has been proven to be a valid and central tool for the understanding of the global radioxenon background.

Atmospheric Transport Modelling

Generally speaking, when particles are being released into the atmosphere, their trajectories are subject to the movement of air masses and other meteorological effects such as precipitation. The concentration is diluted in the atmosphere as the particles are dispersed. When the meteorological data of a certain time period and region are available, the trajectories can be modelled with ATM. By simulating the trajectories of a multitude of particles the dilution of the concentration in the atmosphere can be calculated. The Lagrangian particle dispersion model Flexpart[15] uses a zero acceleration scheme to simulate the particle trajectories, which is accurate to the first order:

$$X(t + \Delta t) = X(t) + v(X, t)\,\Delta t.$$

This equation is used by Flexpart to integrate the particle trajectory equation with $v = v_g + v_t + v_m$ being the wind vector composed of the grid scale wind v_g, the turbulent wind fluctuations v_t and the mesoscale wind fluctuations v_m.

The output of these calculations is the relation between a source and a receptor, which is called the source-receptor sensitivity (SRS).[16] In the case of a single source that is only emitting for the duration of one time step, the total concentration c [Bq/m^3] at the receptor is determined by the source emission S [Bq] multiplied with the source-receptor sensitivity M [m^{-3}], which can be conceived as the volumetric dilution factor:

$$c = MS.$$

For the scenario with multiple sources and/or emission during multiple time steps the total concentration c is calculated by the sum over all sources i

and time steps t:

$$c = \sum_{i,t} MS.$$

When using ATM to determine the time and location dependent SRS the results are stored in a SRS matrix. Flexpart can operate in forward as well as in backward mode.[17] In the case of forward modelling, that is, the dispersion from a source to the environment, for every time step of the simulation all non-zero concentrations on a spatial grid are saved to the SRS matrix. In the case of backward modelling, that is, the determination of all contributions to a sampling period at a fixed location, for every time step all non-zero contributions to the total concentration are saved to the SRS matrix.

For calculating the SRS matrices in this work, Flexpart v8.23 has been applied together with meteorological data from the European Centre for Medium-Range Weather Forecasts (ECMWF). However, M can only account for those conditions that are included in the meteorological data, while local atmospheric patterns that are not resolved by the simulation can lead to altered signals.[18] The meteorological data have a spatial resolution of one degree on a latitude-longitude grid and a time resolution of 3 hours; the data in this analysis had global coverage of the year 2010. For the presented research Flexpart has been applied in the backward modelling mode to determine the SRS matrices for the 39 noble gas stations of the IMS. This has a computational advantage as this scenario has few receptors when compared to the number of radioxenon sources.

Xenon-133 Network Coverage

The purpose of this section is to lay out the approach used in the following to assess the capability of the xenon-133 component of the IMS. The goal is to quantify the effectiveness of the system to detect unusual xenon-133 concentrations in the atmosphere.

So far the term "network coverage" has described the overall ability of the IMS to detect nuclear test explosions. In this work only xenon-133 as the most abundant noble gas isotope is included in the simulations. Previously the spatial distribution of threshold emissions of nuclear explosions that would trigger a detection has been researched.[19] Therefore, a new definition for the xenon-133 network coverage has been established.[20] The network coverage η is the percentage of all possible nuclear explosions, evenly distributed in global space and time that are successfully detected by the IMS.

In the following the network coverage η_{133} denotes the coverage of the IMS xenon-133 component. The exact and real value of this number would only be determined by an infinite number of nuclear test explosions over an infinite time. Here the network coverage is approximated by simulating a multitude n

of nuclear explosions evenly distributed in discrete space and time. For each hypothetical event it is checked whether a detection within the IMS noble gas component is evoked or not. The total share of successfully detected events gives the network coverage:

$$\eta = \frac{n_{detected}}{n_{detected} + n_{undetected}}.$$

When using simulations to approximate the network coverage, certain boundary conditions have to be applied, as the results naturally depend on the chosen parameters:

$$\eta_{reality} \simeq \eta_{simulated}(x_1, x_2, \ldots).$$

In the following these parameters are identified and subsequently determined for the framework of this study. Influencing parameters that were taking into account are:

- Distribution of explosions (spatial and temporal),
- Emissions from explosions,
- Global background from legitimate sources,
- Monitoring network (number and location of monitoring stations); and,
- A detection criterion.

In the following the choice for each parameter is discussed.

Distribution of Explosions

An even spatial distribution of hypothetical nuclear explosions is desired, where no region is a priori weighted in its likelihood to host a nuclear test explosion. The applied ATM runs on a global latitude/longitude grid with a $1^\circ \times 1^\circ$ resolution. The absolute length of a degree of latitude and longitude depends on the radius of a circle of given latitude.[21] Taking the earth as an ellipsoid[22] the arc distance d of one degree can be calculated dependent on the latitude φ as

$$d_{Lat}(\phi) = \frac{\pi r_{eq}\left(1 - e^2\right)}{180\left(1 - e^2 \sin^2 \phi\right)^{\frac{3}{2}}}$$

and

$$d_{Lon}(\phi) = \frac{\pi r_{eq} \cos \phi}{180\left(1 - e^2 \sin^2 \phi\right)^{\frac{1}{2}}}.$$

The latitudinal dependence results in a variation of only up to 1 percent in the absolute length of one degree latitude, i.e., between $d_{Lat}(0^\circ) = 110.57$ km and $d_{Lat}(90^\circ) = 111.69$ km. On the other hand, the degree of latitude results in large variations for the longitude, i.e., from $d_{Lon}(0^\circ) = 111.32$ km over $d_{Lon}(45^\circ) = 78.85$ km to $d_{Lon}(90^\circ) = 0$ km. This means that, if all grid points were treated equally, the spatial density of nuclear explosions would increase from the equator to the poles. Therefore, for circles of latitudes that are higher or lower than the equator only a certain percentage

$$p(\phi) = \frac{\cos\phi}{\left(1 - e^2 \sin^2\phi\right)^{\frac{1}{2}}}$$

of longitudinal grid points have to be considered for hypothetical, nuclear explosions in order to preserve an equally distributed field of events. The remaining grid points are to be equally distributed along each circle of latitude. Instead of $360 \times 179 = 64{,}440$ grid points only a total of $\sum_{\varphi} 360 \times p(\varphi) = 41{,}408$ grid points has to be considered, if one wants to provide an approximately equal spatial distribution. Nevertheless, for precision the underlying ATM, which has been used to determine the SRS matrices of the 39 stations, was still running on the full grid.

For the choice of a certain time period it is reasonable to take a whole year (or multiples of one) in order to balance seasonal variations. For the model time resolution of 3 hours, the course of 1 year and 41,408 grid points a total of $365 \times 8 \times 41{,}408 = 120{,}911{,}360$ hypothetical events are considered.

Emissions from Explosions

As mentioned above only xenon-133 is considered in this approach to determine the network coverage. Due to its fission yield and half-life it is the isotope of choice, when simulating emissions from hypothetical nuclear explosions. Furthermore, it has the best data availability in terms of known emissions from legitimate sources.

For surface explosions it is assumed that the maximum amount of radioxenon from a 10 kt explosion is released within the first time step of the simulation. As discussed above, this means that a source of $S = 10^{16}$ Bq is simulated that releases evenly over the course of one time interval, that is, 3 hours. Underground explosions are considered here with a 1 percent leakage from a 1 kt explosion within the first time interval, i.e., 10^{14} Bq within 3 hours. This emission is assumed where underground explosions are possible, i.e., when the grid point is located above land. Where no solid ground is present, an underwater explosion is assumed. The noble gas release from a 10 kt underwater explosion into the atmosphere is approximated with a release of 10^{16} Bq within one time step due to assumption that the noble gases would raise to the surface without hindrance. In order to be able to distinguish

between underground and underwater events a land/sea-mask has been employed that contains the information for every grid point whether it is above land or sea.

Global Background from Legitimate Sources

The global background of xenon-133 is characterized by a few strong sources (IPFs) and many weak sources (NPPs). In a first step it can be useful to assess the network coverage without any background, and in a second step to include the background. The latter has important effects on choosing a suitable detection criterion. For the background of 2010 the previously discussed emission inventory of five IPFs and 195 NPPs has been included.

Monitoring Network

The current network design foresees 40 IMS stations with noble gas monitoring equipment. Today only the locations of 39 stations have been determined. The 40th station, RNX35, is supposed to be located in India, but is still subject to negotiations. To determine the network coverage today's network with known locations of 39 stations has been considered.

Detection Criterion

In the absence of a radioxenon background the detection criterion is simply that the concentration arriving at the monitoring station must exceed the detector's MDC:

$$c_{ne} \geq MDC.$$

In a scenario including a background the total concentration in a xenon-133 sample is considered as being composed of the legitimate background (bg) and a possible addition from a nuclear explosion (ne):

$$c_{total} = c_{bg} + c_{ne}.$$

Thus, an unusually high total concentration can indicate the presence of xenon-133 from a nuclear explosion. Since the background varies strongly from station to station, a station-specific detection criterion is desirable. A suspicious total concentration in any particular sample is when it is more than one standard deviation (i.e., 1σ) above the mean of c_{bg}, leading to an unbiased and nonetheless station-specific detection criterion:

$$c_{ne} \geq \sigma_{local}.$$

If the contribution from the nuclear explosion is higher than the local standard deviation, it can be contemplated as an unusual high concentration and thus is of interest for further screening. In the following section it is described how the standard deviation has been determined for each station.

Simulation of Xenon-133 Background at IMS Stations

In order to determine the standard deviations, the legitimate background at each of the 39 radioxenon monitoring stations has to be determined. Since some stations are still in planning, under construction or not yet certified, only few stations have been continuously taking data during the last several years. Thus, the main tool to determine the global atmospheric background is ATM. Here it has been applied in backward mode to calculate the SRS matrices of the 39 allocated noble gas monitoring stations. In order to preclude seasonal variations the whole calendar year of 2010 has been considered. Taking into account the 12h/24h sampling time of the stations, this totals approximately 22,000 simulations, each with about 4 hours of CPU time. The calculated SRS matrices were folded with the emission inventory of legitimate background sources in order to derive the time-dependent background xenon-133 concentrations at each station.

Since it is unlikely that the xenon-133 concentration data of one station are normally distributed, the type of mathematical distribution has to be determined. This is necessary to deduct the accordant standard deviation. Included distributions are: Beta, Burr (also known as Singh-Maddala), generalized Pareto, generalized Gamma, inverse Gaussian, Kumaraswamy, log-normal, log-Pearson III, Pearson, Pearson VI, Weibull, and Weibull III.

Each station's simulated data were fitted with these distributions and the results were validated with the Kolmogorov-Smirnov test, the Anderson-Darling test, and the Pearson's chi-squared test. The distributions have been ranked by their goodness of fit according to these three tests. The one distribution with the best average rank was selected. Once the type of distribution has been determined, the standard deviation is calculated.

The results have shown that only a few stations close to IPFs and NPP regions have standard deviation above the MDC. The simulated time series have been compared with available experimental data and have shown good agreement for the regions of North America, Europe, and Oceania, and an underestimation for the region of East Asia.[23] The applied atmospheric transport model Flexpart produces results with little to no bias.[24] Therefore, a possible and likely reason for this is the underestimation of the regional emissions.[25]

Scenarios Overview and Analysis

Three basic scenarios have been developed from the parameters for emissions from nuclear explosions and from background sources: (1) Surface explosions without background, (2) Subsurface explosions without background, and (3) Subsurface explosions with background.[26] Going stepwise from a basic scenario to a more realistic one allows discussion of the changes between the scenarios and helps to understand the impact of the different parameters. For each scenario the network coverage has been calculated on a daily basis

and subsequently averaged over 1 year. Also the spatial distribution has been stored separately for later analysis.

The first scenario with surface explosions includes emissions from nuclear explosions with a full release of xenon-133 into the atmosphere within the first time interval of 3 hours. Due to the assumed absence of the background the detection criterion for a successful detection prescribes that the concentration c_{ne} has to be above the local MDC.

Historically surface nuclear explosions have been detonated in military attacks twice, on 6 August 1945 in Hiroshima and on 9 August 1945 in Nagasaki, and many times during tests. The United States, The Soviet Union, and the United Kingdom stopped atmospheric testing with the entry into force of the Partial Test Ban Treaty (PTBT) in October 1963; France and China stopped by 1974 and 1980 respectively, however, without signing the PTBT. Also peaceful nuclear explosions with full or high leakage rates into the atmosphere are imaginable, e.g., for geoscaping.

This scenario results in an average network coverage of $\eta_{\text{atmo}} = (85.8 \pm 3.5)$ percent. In the simulated year of 2010 the spring season is characterized by values of low global coverages, and the summer season by values of high global coverages. The values of the global coverage have a minimum value of 78.3 percent and a maximum of 92.8 percent. This means that in this scenario of surface explosions the targeted capability of detecting 90 percent of nuclear explosions is not always achieved. In the simulations of the year 2010 it is only achieved during certain short time periods in the summer. However, this reflects the overall value averaged over all locations and time steps. The statistics strongly vary for a certain location or certain regions, e.g., events from location close and, upwind of an IMS station lead more often to detections than locations farther from an IMS station. The spatial distribution for this scenario is shown in Figure 1a.

The meteorological patterns around the equator play a major role in the detection capability. Trade winds carry air masses from lower/higher latitudes towards the equator; Hadley cells keep air masses trapped in loops between the equator and the circles of ± 30 degrees latitudes. The Intertropical Convergence Zone[27] (ITCZ) is a low pressure belt of a few hundred kilometers width close to the equator, where the trade winds collide. This leads to the formation of zones with low air velocities or even windless regions. The transport of air masses to monitoring stations is severely limited in these areas. For latitudes beyond ± 30 degrees the detection probability is clearly higher and more uniformly distributed. The effects of these meteorological patterns, especially in the equatorial region, can be observed in Figure 1a and are identified as the main reason for lowering the total network coverage in this basic scenario.

In the second scenario, subsurface nuclear explosions, underground and underwater, are assumed in the absence of a radioxenon background. Subsurface, nuclear explosions, whether underground or underwater, are more likely

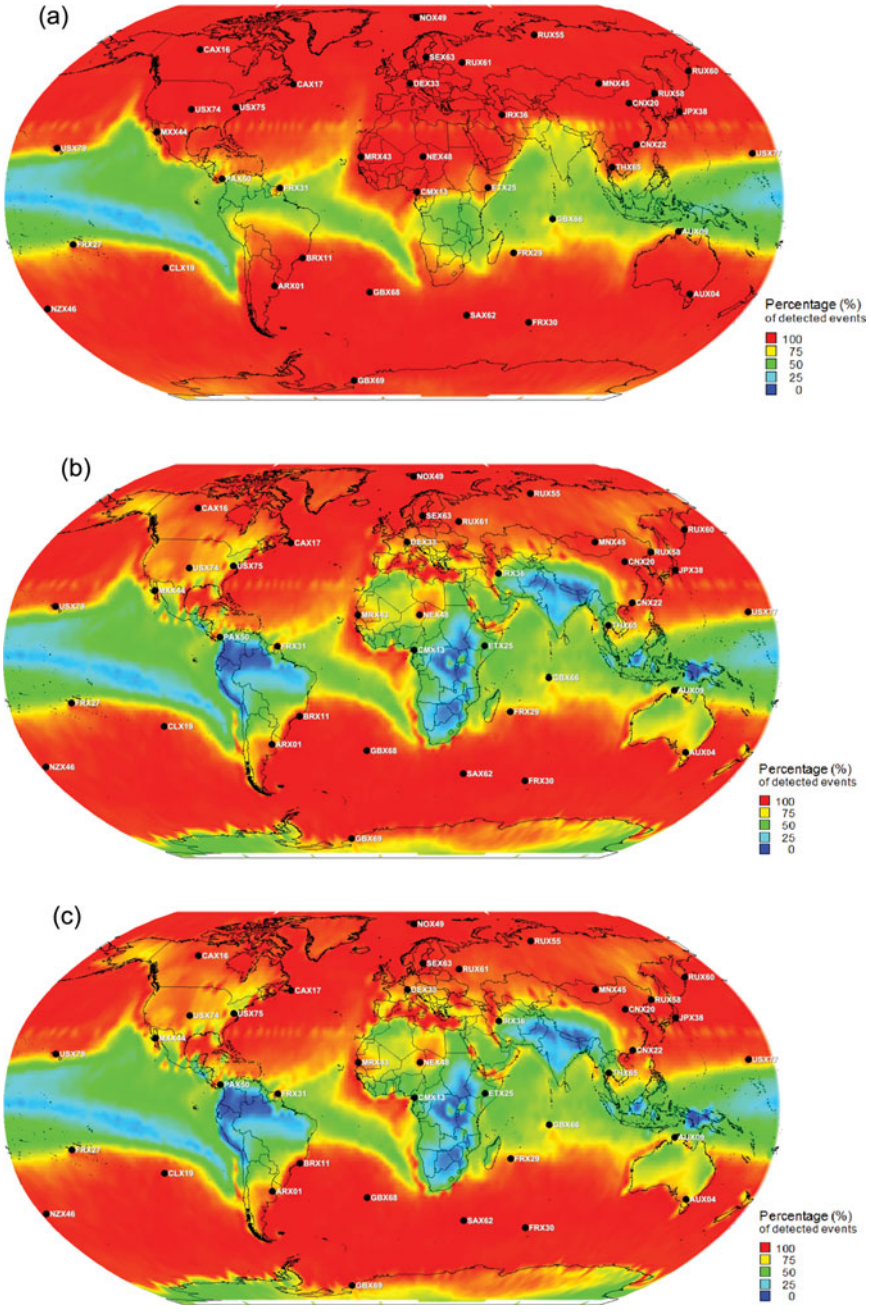

Figure 1: Spatial dependence of network coverage for different scenarios, averaged over one year for each grid point. In each scenario the meteorological patterns surrounding the equator have a major influence. (a) Atmospheric, hypothetical explosions without radioxenon background. (b) Subsurface, hypothetical explosions without radioxenon background. (c) Subsurface, hypothetical explosions including radioxenon background from known, legitimate sources.

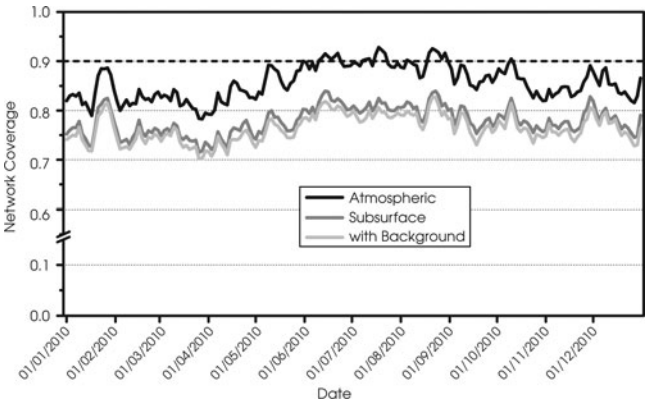

Figure 2: Time series of network coverages for the year 2010. The three scenarios produce time series with very similar characteristics. Moving from above-surface to subsurface explosions reduces the network coverage clearly, while the introduction of the background has an additional (but smaller) negative effect.

to be military tests. As mentioned above, underground nuclear explosions are considered with a 1 percent leakage from a 1 kt explosion within one time interval, while as explained above a full release from a 10 kt explosion is assumed for underwater explosions. However, underwater nuclear explosions are historically rare and would be most likely picked up by the IMS hydroacoustic component, but radioactive proof of such an event is in the scope of the IMS radionuclide and noble gas component. For a successful detection the concentration c_{ne} must exceed the local MDC. Averaged over each day this scenario has a network coverage of $\eta_{subs} = (77.9 \pm 2.8)$ percent. This means that the relocation of nuclear explosions from surface to the subsurface decreases the theoretical network coverage on average by 7.9 percent. The daily values include a minimum of 71.5 percent and a maximum of 84.0 percent. Since the emissions sea-based grid points were kept constant from the previous scenario, the lowered emissions from land-based grid points must be responsible for this decrease. This is seen in Figure 1b, where the distribution over sea-based grid points is the same as for the previously discussed scenario of surface events. The spatial distribution includes again the effects of the ITCZ over large parts of the Atlantic, the Indian, and in particular, the Pacific Ocean. When comparing Figures 1a and 1b nearly all land masses show a reduction in the local detection capability. However, the reduced emissions form subsurface nuclear explosions in equatorial regions together with the peculiar meteorological patterns lead to a clear decrease of the detection probability especially in East Africa, in the northern regions of South America, the Indian Subcontinent, and parts of South East Asia. Additionally to regions with oceanic water also some smaller seas, such as the Mediterranean, the Caspian Sea, or the Great Lakes in Northern America can be identified in Figure 1b via their heightened

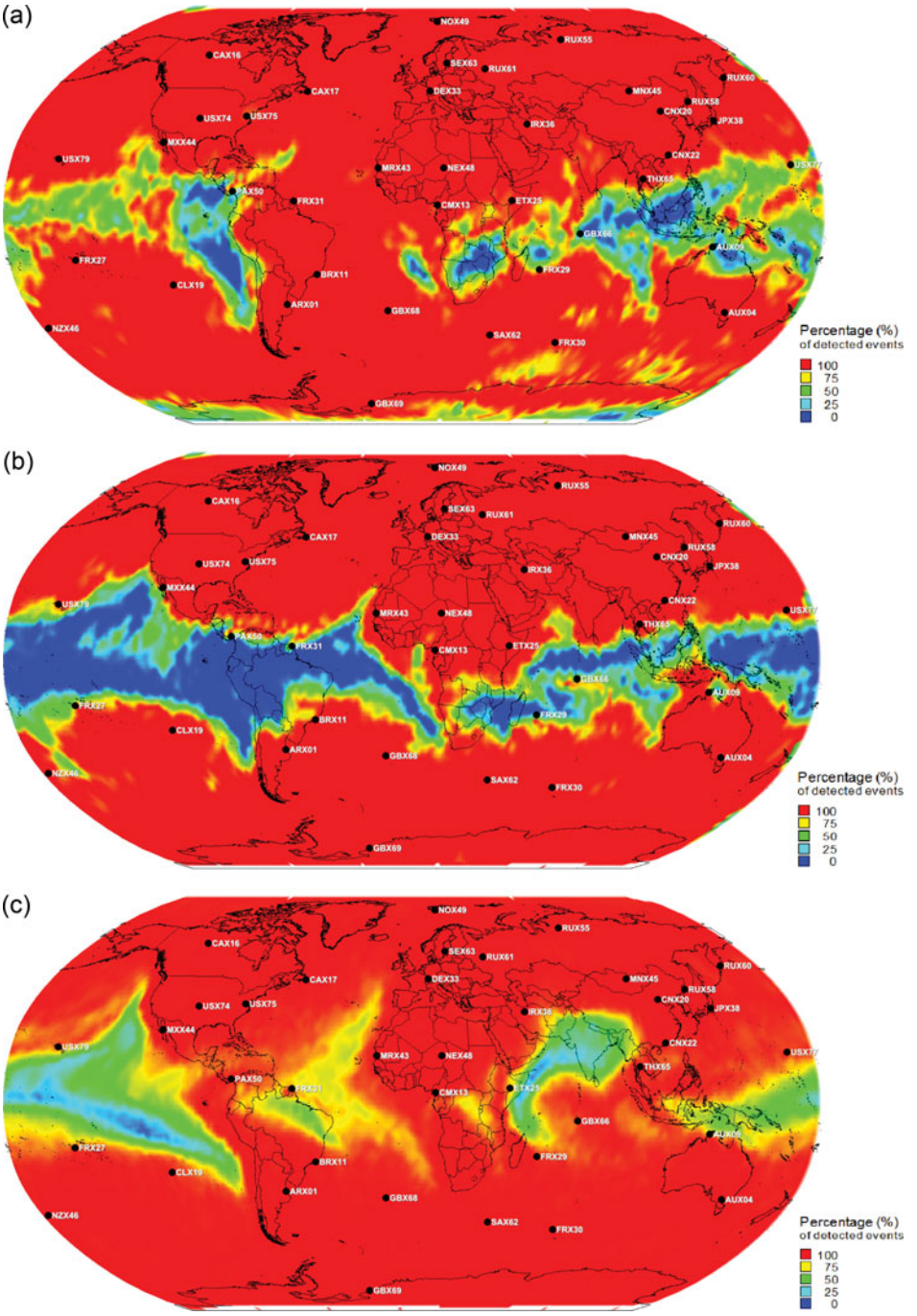

Figure 3: Spatial dependence of network coverage during selected time periods. (a) Heightened network coverage during 23–27 January 2010. (b) Lowered network coverage during 26–30 March 2010. (c) Heightened network coverage during June-August 2010.

detection probability. Their size exceeds the distances between the local grid points.

Thirdly, the most realistic scenario for calculating the network coverage is not only to assume subsurface explosions where possible, but also to take into account the global background. When including the radioxenon background, as discussed above, a detection of radioxenon does not necessarily imply the occurrence of a nuclear explosion. The existence of a background results in the detection criterion that the concentration c_{ne} must exceed the local standard deviation. For stations with a standard deviation below the MDC the former criterion of c_{ne} exceeding the MDC is still valid. The application of this stricter detection criterion results in a lowered global network coverage of $\eta_{subs+bg} = (76.4 \pm 2.8)$ percent. The time series of daily values include a minimum of 70.2 percent and a maximum of 82.7 percent. As to be expected, the further reduction is mainly caused by reduced detection capabilities for events in Northern America and Western Europe (see Figure 1c). This is due to the regional higher density of NPPs and IPFs. Surprisingly events in East Asia that are likely to be detected by JPX38 in Japan are not negatively affected by the regional background from NPPs. However, previous research suggests that the applied radioxenon emission inventory may generally and regionally be underestimated.[28] Thus the real impact might be higher in certain regions and result in a further decrease of the total network coverage.

However, expressing the network coverage in a single value neither embraces the contrast between regions nor the variability in time.

Spatial and Time Dependence Analysis

Seasonal Dependence

The general time dependence over the course of 1 year is very similar for all three of the above scenarios. As seen in Figure 2 they share most characteristic peaks on a day-to-day basis, e.g., the positive peak at the end of January 2010, and also medium-term developments, for example, the high plateau between June and August 2010. Large parts of the areas with low detection probability are found in the tropical Pacific. This part of the world is not only subject to the aforementioned trade winds, but also to the El Niño and La Niña oscillations.[29] El Niño is most notably marked by an increased surface temperature of the western Pacific, and La Niña by lowered surface temperature of the equatorial eastern Pacific, both with temperature differences of at least ± 0.5K. In the contemplated year 2010, the maximum surface temperature differences were ± 1.5K with regard to the average.[30] The effects, however, can be globally observed with impact on atmospheric pressure in the Indian Ocean, on trade winds in the south Pacific, and on general climate, e.g., also in Europe and Africa. In the year 2010 El Niño peaked during January and ended in March,

while from April to July the surface temperatures normalized. From August onwards for the rest of the year La Niña was predominant. These time periods correlate with the general development of the coverage over the year.

In the following, three selected time periods from the third scenario (subsurface + background) are analyzed due to their special characteristics. During the last third of January 2010 the network coverage exhibits a 5–7 days positive peak with a maximum value of about 10 percent above the previous and following local minima, as seen in Figure 2. The spatial relocation of the network coverage is shown in Figure 3a. It is seen that the equatorial zones with typical low detections have contracted. El Niño peaked in January and the turning point of the surface temperature might have had an effect on the transport mechanisms in the Pacific.

The spatial distribution of the minimum of the network coverage from 26 to 30 March has been plotted in Figure 3b. It is seen that the zones of lower detection probability are still connected, having an extremely low detection probability of down to 0 percent in wide areas, and cover significantly larger areas than on average. The spatial distribution of detection probabilities of the network coverage's high plateau from June to August 2010 has been plotted separately in Figure 3c. When comparing this 3-month period with the annual distribution in Figure 1a, it is seen that the higher probability between June and August 2010 is due to a different distribution of the equatorial meteorological patterns; the low-probability zones around the equator are smaller and even clustered, i.e., separated from each other by zones of high detection probability.

This change of detection probabilities is believed to be caused by a particular behavior of the ITCZ. During these months, that is, during the Northern summer, the ITCZ tends to move farther away from the equator and thus allows hypothetical emissions to be more effectively transported. This meteorological behavior of the ITCZ is generally not observed during Southern summers (Northern winter), which is congruent with the generally lower simulated detection probability from January to March 2010, as seen in Figure 2. Furthermore, the occurrence of La Niña during these months may have influenced the detection capability, especially for events in the Pacific area.

It is summarized that the seasonal dependence of the network coverage can likely be attributed to meteorological effects around the equator and to the seasonal dependence of transport mechanisms of the ITCZ.

Spatial Dependence

As seen from Figure 1c a high detection probability exists for wide areas even for the subsurface/background scenario. As seen in Figure 4 the frequency analysis shows a clear peak for detection rates above 90% percent. However, if considering only the set of land-based grid points, the relative occurrence of

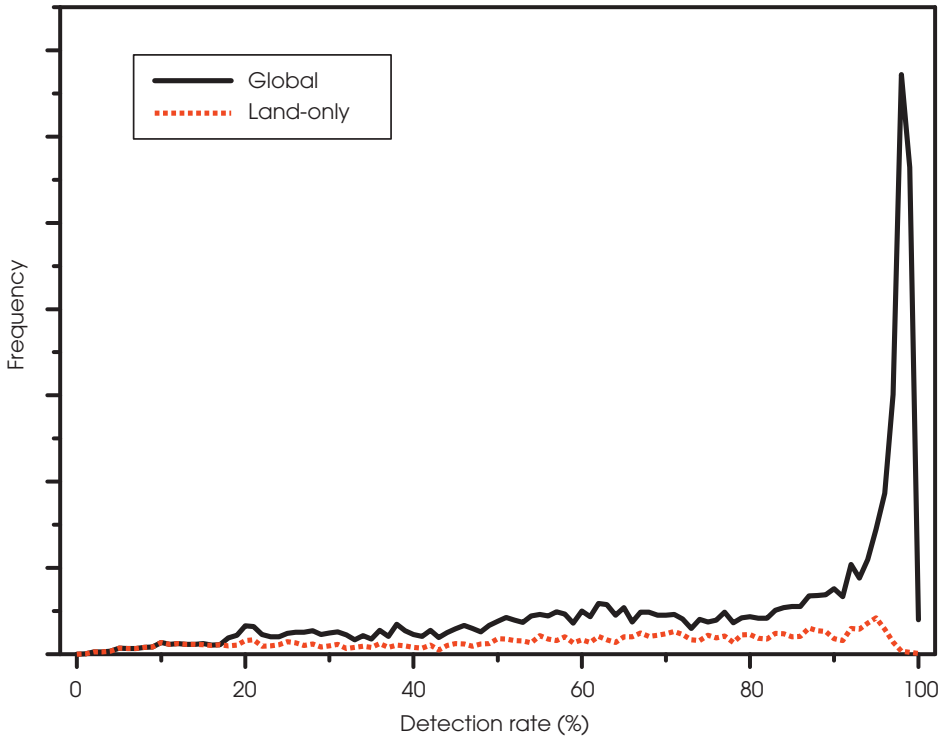

Figure 4: Occurrence of grid points depending on the detection rate for the subsurface scenario including the background. Land-based grid points have a lower occurrence of high detection rates of above 90%.

such high detection probabilities is clearly reduced. This reduction is caused by the assumed leakages of 100 percent for underwater and 1 percent for underground events. The difference is further amplified by the larger number of water-based grid points as 71 percent of the globe is covered by water.

The events from sea-based grid points tend to have high detection rates in all scenarios. The differences of η in the three described scenarios are caused rather by a changing detectability of land-based events. If, for example, assuming a scenario with a secretly conducted nuclear test, it is more likely that this event will be underground. Therefore, it can be a reasonable consideration to handle the land-based network coverage separated from the total network coverage. In this case the network coverages of the three scenarios are shifting from the previous values:

$$\eta_{\text{atmo;land}} = 91.1\%(+),$$
$$\eta_{\text{subs;land}} = 64.4\%(-),$$
$$\eta_{\text{subs+bg;land}} = 60.2\%\,(-).$$

In parentheses it is indicated whether the land-based coverage is higher or lower in comparison to the global coverage. For the surface-event scenario without background the land-mass network coverage is 5.3 percent higher than the total network coverage. This is caused by the fact that the global distribution of low detection rates is mainly found on the Pacific Ocean, i.e., on grid points above sea, and that the emissions of the land-based events are in most cases strong enough to be detected. When moving to the scenario of subsurface events without background the network coverage is 13.5 percent less than for all events combined. This means that the land-based network coverage is sensitive to the assumed emission (or leakage) from underground tests. Also the coverage for the background scenario is smaller by 16.2 percent when compared to the global value, indicating that land-based events are more impacted by the radioxenon background than sea-based events. This is plausible because the radioxenon emitters are found on land and are affecting nearby stations.

Non-Detectable Events

Previously the seasonal as well as the spatial dependencies of detections have been discussed. In order to understand the parameters influencing the network coverage it is necessary to also discuss the spatial distribution of the non-detections. In the above-described simulations of hypothetical nuclear explosions an event can remain undetected due to the following two factors:

1. The activity concentration arriving at an IMS noble gas station does not fulfil the necessary detection criteria; or,
2. The plume of the emissions from the event does not reach any IMS noble gas station within the simulation time of 14 days.

In cases of (1.) the emission strength and/or the leakage of radioxenon versus the legitimate background is the main factor in determining whether the event can be detected or not. In cases of (2.) the simulations predict that the radioxenon emissions of the event will stay undetected in any case within the simulation time of 2 weeks, i.e., they are non-detectable independent of their emission strength.

For every grid point, for which explosions have been assumed, the number of non-detections due to (2.) is counted for the whole time period. Scaled to the total number of simulated events per grid point, the percentage of non-detectable events is calculated for each grid point. This results in a total percentage of non-detectable events of 13.2 percent. Naturally, this value is independent of the leakage and the background, and therefore identical for all three of the presented scenarios. The global distribution is plotted in Figure 5, where it is observed that the spatial distribution is very similar to that of the

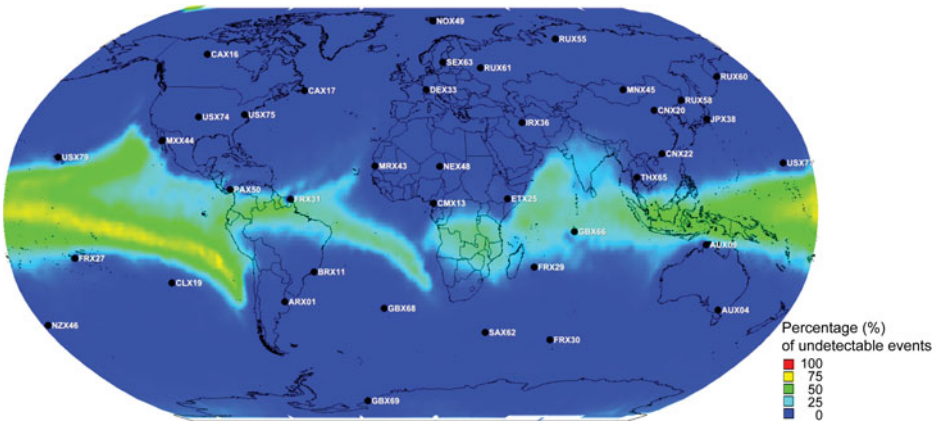

Figure 5: Probability distribution of non-detectable events where emissions do not reach the IMS noble gas component. The spatial distribution is very similar to the scenario shown in Figure 1a, where the meteorological patterns surrounding the equator are mostly responsible for the characteristics.

basic, surface explosion scenario presented in Figure 1a. Taking into account the total network coverage for the surface scenario of 85.8 percent and the share of non-detectable events of 13.2 percent, only 1 percent of the above-surface events did not evoke a detection due to the emission strength being too small. The analogue calculation for subsurface events without background results in a share of 8.9 percent of events that are in principle detectable by today's network (10.4 percent for subsurface events with additional background). In these cases one or a combination of the following factors prevents detection: too low emission strength, too high atmospheric dilution and/or too high detection criteria.

The global impact of the legitimate radioxenon background seems rather small, but on a regional scale it can have significant effects as seen when comparing the land mass of North America in Figures 1b and 1c. However, the presented approach treats by definition all grid points equally, including points above sea. In a CTBT scenario of a secret (or faked) nuclear test, one might be more interested in land-based and especially underground scenarios.

Table 1 gives an overview over how the network coverage changes for the three different scenarios for land and sea-based events. Additional to the network coverage, also the shares of non-detectable and not-detected events are listed. For land-based events the percentage of non-detectable events is reduced to 5.9 percent.

According to Figure 5, these events are also located in equatorial regions and are results of the typical meteorological patterns. The remaining share of events that have not been detected is due to the fact that the concentrations that arrive at the receptor have not been identified as unusually high. This

Table 1: Network coverages and shares of non-detections for global, land-based and sea-based events.[1] Non-detectable events have emissions that do not reach an IMS noble gas station within 14 days. The remaining share denotes events (not detected), for which a simulated emission reaches at least one IMS noble gas station, but does not fulfil the detection criteria, i.e. the concentration is too low.

	Scenario	Surface (%)	Subsurface (%)	With background (%)
Total	Network coverage	85.8	77.9	76.4
	Non-detectable	13.2	13.2	13.2
	Remaining	1.0	8.9	10.4
Land	Network coverage	91.1	64.4	60.2
	Non-detectable	5.9	5.9	5.9
	Remaining	3.0	29.7	33.9
Sea	Network coverage	83.5	83.5	83.0
	Non-detectable	16.2	16.2	16.2
	Remaining	0.3	0.3	0.8

Note. [1]As discussed earlier, a release of 10^{16} Bq of xenon-133 is assumed for surface (land-based) and all sea-based explosions and 10^{14} Bq of xenon-133 is assumed for underground (land-based) explosions to emphasize the difference between tests with low and high releases, and their influence on the global coverage. As seen in Figure 5 even the coverage of sea-based events with their higher emissions suffers predominantly from the emissions not reaching an IMS station.

share of not-detected events clearly rises to about 30 percent for subsurface scenarios with and without background. This leads to a network coverage of 60.2 percent for the scenario of land-based, subsurface explosions and existing background. The network coverage for sea-based events remains almost constant and shows only a low dependence on the radioxenon background. The major part of the not detected, land-based events is found in equatorial regions of South America, Africa, and India, as seen when comparing Figure 1a to 1c. For the subsurface-with-background scenario these regions are tending to have a detection capability of 25 percent or even significantly below. Large parts of the landmasses of North America are affected by a less significant, but more uniformly and more evenly distributed loss in the detection capability due to the high number of radioxenon emitters.

The share of non-detectable events and its spatial distribution can only be overcome with additional IMS noble gas stations. Additional stations would decrease the average distance between CTBT-relevant events and noble gas stations, and therefore also decrease the dilution factor. This would increase the relative impact of such events on the legitimate radioxenon concentration at noble gas stations. On the other hand, the detection probability for events that are in reach of a monitoring station, but are not detected due to non-fulfilled detection criteria, can be potentially improved by additional noble gas stations, a sophisticated categorization scheme (to decide whether or not a sample signifies a detection), and a reduction of the legitimate radioxenon background.

Global Coverage

From the beginning the IMS has been designed to evenly cover the world's surface without any focus or emphasis on areas such as former nuclear test sites. In order to reach this goal the monitoring stations have been scattered more or less uniformly over the globe. Due to the more uniform dispersion of waves in the earth, the ocean and the atmosphere the equal coverage can be fulfilled more easily for the waveform technologies than for the radionuclide monitoring network. As it has been shown the effectiveness of the latter is subject to non-uniform meteorological patterns. The distribution of stations contradicts the distribution of wind patterns and station density should be increased in equatorial regions. Known test cases for the IMS have been the three North Korean nuclear tests in 2006, 2009, and 2013. While the tests were announced by the North Korean government, all three were seismically detected. Furthermore, in May 2010 multiple IMS stations in South East Asia picked up traces of various radionuclides and noble gases.[31] However, the source type and source location of those detections is still subject to controversy. A nuclear test or accident in the North Korean region cannot be excluded, while detections from a South Korean non-IMS station improved the backtracking capability.

For the test of 2006 with a yield of 0.65–1.1 kt the closest downwind station, in Takasaki, Japan, was not operational, but suspicious concentrations of xenon-133 were detected in Yellowknife/Canada.[32] For the test of 2009 with a yield of 1.5–4.5 kt, though stronger than the previous test and with the Japan station operating, no noble gases have been detected. For the test of 2013 with a yield of 6–9 kt concentrations of radioxenon were only detected about six weeks after the test.[33] In contrast to this the network coverage shows a high probability to detect emissions from this region. The containment of noble gases in the cavity of the explosion seems to play the most important role in the three cases of North Korean tests. This means that successful detection is not only dependent on the atmospheric transport, the detection system, and the background, but also highly dependent on the leakage from the underground into the atmosphere.

Beyond this, the coverage of other states is of interest, with special emphasis on the Annex-2 states; of scientific interest to provide a global coverage and of political interest for the forthcoming CTBT ratification process. The following Annex-2 states have significant regions within their borders with an annual detection average of less than 50 percent: Algeria, Argentina, Australia, Bangladesh, Brazil, Canada, Chile, China, Colombia, Congo, Egypt, India, Indonesia, Iran, Mexico, Pakistan, Peru, Spain, South Africa, and the United States.

Though some states, for example, the United States, are affected by the radioxenon background, in most cases the meteorological patterns are the main cause. The future coverage of the Indian subcontinent will depend on

the location of the planned monitoring station. However, the difficulties of a reliable verification regime are used by some countries as an argument against the ratification of the CTBT.[34] Thus, these regional blind spots of the IMS noble gas component could affect the position of states towards the CTBT in various ways. First, it supports the arguments against the ratification of the CTBT. Second, the existence and location of these blind spots could potentially motivate affected states to keep open an option for a nuclear weapons program. Thus, it is of importance and in the interest of a verifiable CTBT to extend the number of noble gas monitoring stations.

It is recommended to add more stations, especially in equatorial areas, to account for meteorological patterns. Any further regional extensions of the noble gas monitoring network would also depend on the further global growth in background radioxenon.

Summary and Recommendations

The IMS noble gas stations have been distributed more or less evenly across the globe and as a result do not account for the meteorological transport processes in the equatorial region. Therefore, blind spots exist, lowering the detection probability of nuclear explosions. Furthermore, the distribution of legitimate radioxenon emitters, which follows mainly economic factors, has not been taken into account. These facilities have clearly a negative, but more regional than global, impact. This means that an IPF can noticeably decrease the coverage in downwind regions, but the net impact on the global coverage of the Earth's surface including the oceans is minor. However, due to the economic nature of the medical isotope market the number of emitters and their releases will certainly change over time. Accordingly the impact on the detection capability will change regionally. Therefore, it is of significant interest for an effective and stable noble gas detection capability to reduce or at least maintain the existing background, which is mainly created by IPFs. In the interest of the treaty it is desirable that new facilities follow a proposed emission maximum, e.g., 5 GBq/day.[35] This guideline is easier to implement for upcoming facilities than for existing ones. The latter have little reason to make costly changes to already state-approved processes within their facility, which do not stand in contradiction to any respective law.

Further improvement is possible by better understanding the noble gas background and more sophisticated detection criteria, e.g., including isotopic ratios and/or time series analysis.

However, at the moment the biggest enhancement of the noble gas component could be gained by adding more stations in certain equatorial regions. The issue of emissions that do not reach a monitoring station within the simulation time of 2 weeks negatively affects the IMS noble gas component in its purpose to prove the nuclear character of an event. In such a scenario one would have to rely on other means of verification, such as waveform technologies, on-site

inspections and/or diplomatic clarification. The noble gas component has not reached its full potential and will benefit from additional stations.

FUNDING

The authors gratefully acknowledge the support by the National Scientific Committee Technology of National Institute of Nuclear Physics for the Environmental Radioactivity Monitoring for Earth Sciences (ERMES) project. The authors are grateful to the computer lab of the Italian National Institute of Nuclear Physics and to the Department of Mathematics and Physics of the Roma Tre University. Station and sampling data have been kindly provided through the virtual Data Exploitation Centre (vDEC) within the framework of an agreement between the CTBTO and the Department of Mathematics and Physics at Roma Tre University. The atmospheric transport modeling has been accomplished with meteorological data provided by the European Centre for Medium-Range Weather Forecasts under a collaboration agreement with the Department of Mathematics and Physics at Roma Tre University.

NOTES AND REFERENCES

1. Joachim Schulze, Matthias Auer, and Robert Werzi, "*Low Level Radioactivity Measurement in Support of the CTBTO*," *Applied Radiation and Isotopes*, 53 (2000): 23–30.

2. Ola Dahlman, Svein Mykkeltveit, Hein Haak, Dahlman, Ola, Svein Mykkeltveit, and Hein Haak, *Nuclear Test Ban: Converting Political Visions to Reality* (Berlin: Springer, 2009).

3. Martin Kalinowski, "Characterisation of Prompt and Delayed Atmospheric Radioactivity Releases from Underground Nuclear Tests at Nevada as a Function of Release Time," *Journal of Environmental Radioactivity*, 102 (2011): 824–836.

4. Martin Kalinowski and Matthias Tuma, "Global Radioxenon Emission Inventory Based on Nuclear Power Reactor Reports," *Journal of Environmental Radioactivity*, 100 (2009): 58–70; Gerhard Wotawa, Andreas Becker, Martin Kalinowski, Paul Saey, Matthias Tuma, and Matthias Zaehringer, "Computation and Analysis of the Global Distribution of the Radioxenon Isotope 133-Xe based on Emissions from Nuclear Power Plants and Radioisotope Production Facilities and its Relevance for the Verification of the Nuclear-Test-Ban Treaty," *Pure and Applied Geophysics*, *167*(2010): 541–557.

5. Matthias Auer, Timo Kumberg, Hartmut Sartorius, Bernd Wernsperger, and Clemens Schlosser, "Ten Years of Development of Equipment for Measurement of Atmospheric Radioactive Xenon for the Verification of the CTBT," *Pure and Applied Geophysics*, 167 (2010): 471–486.

6. A thallium-doped sodium iodide scintillation detector.

7. *Ten Years of Development of Equipment*, 471–486.

8. Paul Saey, Theodore Bowyer, and Anders Ringbom, "Isotopic Noble Gas Signatures Released from Medical Isotope Production Facilities—Simulations and Measurements," *Applied Radiation and Isotopes*, 68 (2010): 1846–1854.

9. *Global Radioxenon Emission Inventory*, 58–70.

10. Paul Saey, "The Influence of Radiopharmaceutical Isotope Production on the Global Radioxenon Background," *Journal of Environmental Radioactivity*, 100 (2009): 396–406.

11. *Workshop on Signatures of Medical and Industrial Isotope Production*, organized by Pacific Northwest National Laboratory in Strassoldo, Italy, 12–17 June 2011 and 18–22 June 2012.

12. Personal communication with Benoit Deconninck (National Institute for Radioelements, IRE) and Emmy Hoffmann (Australian Nuclear Science and Technology Organisation, ANSTO).

13. *Global Radioxenon Emission Inventory*, 58–70.

14. Power Reactor Information System (PRIS) by the IAEA, available at www.iaea.org/programmes/a2/.

15. Andreas Stohl, Harald Sodemann, Sabine Eckhardt, A. Frank, Petra Seibert, and Gerhard Wotawa, "The Lagrangian Particle Dispersion Model Flexpart version 8.2," available at http://flexpart.eu.

16. Gerhard Wotawa et al., "Atmospheric Transport Modelling in Support of CTBT Verification—Overview And Basic Concepts," *Atmospheric Environmen*t, 37 (2003): 2529–2537.

17. *Atmospheric Transport Modelling in Support of CTBT Verification*, 2529–2537.

18. Wolfango Plastino, Romano Plenteda, Georgio Azzari, Andreas Becker, Paul Saey, and Gerhard Wotawa, "Radioxenon Time Series and Meteorological Pattern Analysis for CTBT Event Categorisation," *Pure and Applied Geophysics*, 167 (2010): 559–573.

19. *Computation and Analysis of the Global Distribution of the Radioxenon Isotope*, 541–557.

20. Michael Schöppner, "Analysis of the Global Radioxenon Background with Atmospheric Transport Modelling for Nuclear Explosion Monitoring," Ph.D. thesis at the University of Roma Tre, 2012.

21. Peter Osborne, "The Mercator Projections," Edinburgh, 2008, http://www.mercator99.webspace.virginmedia.com/mercator.pdf.

22. The earth is taken as an ellipsoid with equatorial radius $r_{eq} = 6{,}378$ km, polar radius $r_{pol} = 6{,}357$ km and eccentricity $e^2 = r^2_{eq} - r^2_{pol}/r^2_{eq} = 6.57 \times 10^{-3}$.

23. *Analysis of the Global Radioxenon Background*.

24. Andreas Stohl, M. Hittenberger, and Gerhard Wotawa, "Validation of the Lagrangian Particle Dispersion Model Flexpart Against Large-Scale Tracer Experiment Data," *Atmospheric Environment*, 32 (1998): 4245–4264.

25. *Computation and Analysis of the Global Distribution of the Radioxenon Isotope, 541–557; Analysis of the Global Radioxenon Background*.

26. *Analysis of the Global Radioxenon Background*.

27. The Intertropical Convergence Zone (ITCZ) is an equatorial area of a few hundred kilometres width and characterised by persistent convergence of air masses. The associated clouds can build up into the tropopause. The location of the ITCZ depends on the season of the year. From January to July it moves northwards. In northern and southern direction of the ITCZ the trade winds are the predominant wind patterns.

28. Blake Orr, Michael Schöppner, Rick Tinker, and Wolfango Plastino, "Detection of Radioxenon in Darwin, Australia Following the Fukushima Dai-ichi Nuclear Power Plant Accident," *Journal of Environmental Radioactivity*, 126 (2013): 40–44;

M. Schöppner, M. Kalinowski, W. Plastino, A. Budano, M. Vincenzi, A. Ringbom, F. Ruggieri, and C. Schlosser, "Impact of Monthly Radioxenon Source Time-Resolution on Atmospheric Concentration Predictions," *Pure and Applied Geophysics*, *171*(2014): 699–705; *Computation and Analysis of the Global Distribution of the Radioxenon Isotope*, 541–557.

29. El Niño, and La Niña are quasi-periodic meteorological patterns occurring across the tropical Pacific.

30. National Oceanic and Atmospheric Administration, Climate Prediction Center of the National Centers for Environmental Prediction, "ENSO Cycle: Recent Evolution, Current Status and Predictions," http://www.cpc.ncep.noaa.gov/products/analysis_monitoring/lanina/enso_evolution-status-fcsts-web.pdf, 2012.

31. L.-E. De Geer, "Radionuclide Evidence for Low-Yield Nuclear Testing in North Korea in April/May 2010," *Science & Global Security*, 20 (2012): 129; G. Wotawa, "Meteorological Analysis of the Detection of Xenon and Barium/Lanthanum Isotopes in May 2010 in Eastern Asia," *Journal of Radioanalytical and Nuclear Chemistry, 296*(2013): 339–347; C. M. Wright, "Low-Yield Nuclear Testing by North Korea in May 2010: Assessing the Evidence with Atmospheric Transport Models and Xenon Activity Calculations," *Science & Global Security, 21*(2013): 3–52.

32. Anders Ringbom, Klas Elmgren, K. Lindh, Jenny Peterson, Theodore Bowyer, James Hayes, Justin McIntyre, M. Paninsko, and R. Williams, "Measurements of Radioxenon in Ground Level Air in South Korea Following the Claimed Nuclear Test in North Korea on October 9, 2006," *Journal of Radioanalytical and Nuclear Chemistry*, 282 (2009): 773–779.

33. Anders Ringbom et al., "Radioxenon Detections in the CTBT International Monitoring System Likely Related to The Announced Nuclear Test in North Korea on February 12, 2013," *Journal of Environmental Radioactivity*, 128 (2014): 47–63.

34. Katarzyna Kubiak, "CTBT Hold-out States. Why did the Longest Sought, Hardest Fought Prize in Arms Control History Still Not Enter Into Force?" Institute for Peace Research and Security Policy at the University of Hamburg, IFAR Working Paper No. 16, June 2011.

35. Harry Miley, Theodore Bowyer, Paul Eslinger, Rosara Kephart, and Paul R. J. Saey, "Releases from Medical Isotope Production Facilities and Their Effect on Monitoring Nuclear Explosions," Workshop on Signatures of Medical and Industrial Isotope Production, Strassoldo, Italy, 2012.